https://doi.org/10.5194/wes-2025-231
Preprint. Discussion started: 8 December 2025

eawe european academy of wind energy
Open Access WIND ENERGY SCIENCE DISCUSSIONS

Calibration and validation of an engineering model for vortex induced vibration prediction in wind turbine towers

Dimitris Vlastos[1], Niki Tzimi[1], Georgia Trampa[1], Vasilis Riziotis[1], Dimitris Manolas[2], Nikos Spyropoulos[1]

[1] School of Mechanical Engineering, National Technical University of Athens, Athens, 15780, Greece
[2] iWind Renewables, PC, Gerakas, 15344, Greece

Correspondence to: Dimitris Vlastos (dvlastos@fluid.mech.ntua.gr)

Abstract. The prediction of vortex-induced vibrations (VIV) caused by vortex shedding downstream of wind turbine towers is a complex and challenging engineering problem for wind turbine manufacturers. These vibrations typically occur when the turbine is in parked or idling mode, or during the installation and commissioning phases. The paper reviews the current engineering framework for predicting VIV in wind turbine towers, with a focus on models that can be integrated into comprehensive aeroelastic design tools. It further explores the application of the Hartlen-Currie lift oscillator model as a predictive tool for VIV in tower structures. In the paper, the free parameters of the Hartlen-Currie model are properly calibrated versus experimental results for elastically mounted, rigid untapered cylinders with the aim to capture the vibration amplitudes in the occurrence of lock-in events and the wind velocity at which the onset of lock-in (maximum vibration amplitude) is obtained. Once calibrated, the model is applied to simulate VIV in an elastic, cantilevered cylinder. The results for both simply supported and cantilever configurations are then compared with experimental measurements and predictions from other widely used engineering models in the literature. The governing equations are expressed in a non-dimensional form to facilitate the calibration of the model's defining parameters. Comparisons with wind tunnel measurements show that the proposed model is capable of successfully predicting the maximum vibration amplitudes and the onset velocity of VIV.

1 Introduction

VIV in wind turbine towers present a well-known challenge for wind turbine manufacturers (Veers et al., 2023). Numerous cases of excessive and often "unexpected" vibrations have been reported during the installation and commissioning phases - prior to electrification - as well as when turbines are parked or idling at low speeds. These vibrations are frequently attributed to fluctuating wind loads acting on the cylindrical tower, resulting from vortex shedding in its wake. It is noted that in some cases, vortex shedding originating from the blades can also induce unsteady aerodynamic loads and lead to VIV in the wind turbine structure (Horcas et al., 2022; Zou et al., 2014) but such vibrations are not within the scope of the present study. During VIV, substantial vibration amplitudes can develop within seconds across various components of the wind turbine, ultimately leading to limit cycle oscillations.

https://doi.org/10.5194/wes-2025-231
Preprint. Discussion started: 8 December 2025

eawe european academy of wind energy
Open Access WIND ENERGY SCIENCE DISCUSSIONS

When the vortex shedding frequency approaches a natural frequency of a tower mode, a dynamic interaction occurs between the unsteady flow and the tower's elastic response - known as lock-in. The lock-in phenomenon is experienced by the turbine as a synchronization between its structural vibration frequency and the periodic aerodynamic excitation caused by the flow around the tower. VIV due to tower vortex shedding can occur under several conditions: (a) on the bare tower, before the Rotor-Nacelle Assembly (RNA) is installed, (b) on partially assembled RNAs—with none, one, or two blades mounted, or (c) on the fully assembled turbine when the rotor is parked or rotating slowly in idling mode. It is important to note that tower vortex shedding can occur under all inflow conditions. However, during normal operation, rotor rotation enhances wake mixing, thereby disrupting coherent vortex structures and mitigating VIV.

For typical onshore and offshore wind turbines, once the Rotor-Nacelle Assembly (RNA) is installed, the vortex shedding frequency of the tower often aligns with the first bending mode frequency of the structure at low to moderate wind speeds, typically in the range of 5–15 m/s. In contrast, when the RNA is not yet installed, the lock-in phenomenon tends to occur at higher wind speeds. In addition, onshore wind turbine manufacturers sometimes modify tower designs—particularly in terms of height and diameter - to better harness site-specific wind resources. For example, taller towers are often used at low-wind sites to access stronger wind flows at higher altitudes. In such cases, where towers can be up to 50% taller than standard configurations, the vortex shedding frequency may approach the second bending mode frequency of the tower, typically at wind speeds between 15–20 m/s. In both scenarios - whether due to the absence of the RNA or the use of tall towers - the elevated lock-in wind speeds result in larger aerodynamic excitation forces, which in turn cause more severe structural vibrations. A common feature in all these cases is that during lock-in, high-amplitude oscillations develop in the crossflow direction - the direction with the lowest aerodynamic damping - greatly accelerating fatigue damage and potentially compromising the structural integrity of the wind turbine.

The prediction of wind turbine loads and vibration amplitudes during tower lock-in events primarily relies on the engineering framework established by the Eurocode standard (European Committee for Standardization (CEN), 2005; Manolas et al., 2022). According to this standard, the effects of vibrations induced by vortex shedding are represented as a periodic inertial force distribution along the height of the tower, acting perpendicular to the wind direction. This force is dependent on the tower's linear mass distribution, the frequency and mode shape of the excited structural mode, and the maximum vibration displacement amplitude, which can be determined using two alternative approaches provided in the standard.

Engineering models in the literature are commonly classified according to how they represent the fluid forcing term, which in turn determines the degrees of freedom in the mathematical formulation (Fernandez-Aldama et al., 2024). In this work, we specifically distinguish between models based on whether they incorporate an explicit oscillator equation for the lift force.

A first class of alternative engineering models explored in the literature incorporate additional nonlinear aeroelastic force components into the sinusoidally varying lift force induced by vortex shedding around the cylindrical tower. These additional terms typically include a component in phase with the structural motion (aerodynamic stiffness) and/or a nonlinear

https://doi.org/10.5194/wes-2025-231
Preprint. Discussion started: 8 December 2025

eawe european academy of wind energy
Open Access WIND ENERGY SCIENCE DISCUSSIONS

component in quadrature with the motion velocity (aerodynamic damping). For an elastically supported rigid cylinder, such models are commonly expressed as single-equation formulations, where the nonlinear stiffness and/or damping forces are introduced as external excitations into the one-degree-of-freedom dynamic motion equation. Representative models of this type include those proposed in the literature (Basu and Vickery, 1983; Magnus et al., 2013; Scanlan, 1981). Although the aforementioned models can effectively predict the maximum vibration amplitude occurring during lock-in, they are unable to provide detailed information of the distribution of the self-excitation power within the lock-in region and to predict the wind speed at which the onset of lock-in appears (wind velocity within the lock-in region at which maximum vibration amplitude takes place). A critical review of the above models can be found in (Lupi et al., 2018). In the above reference, prediction improvements are proposed for one equation models, based on the results from wind tunnel experiments on a rigid cylinder undergoing imposed periodic motions.

A second class of engineering models investigated in the literature involves representing the aerodynamic excitation - specifically the lift force - through the solution of a second-order oscillator equation. A representative example of this type is the Hartlen and Currie model (Hartlen and Currie, 1970). For a rigid elastically supported cylinder, these models are formulated as coupled systems of two equations (and thus two state variables): the first is the structural dynamic equation of motion, and the second is the oscillator equation that governs the evolution of the lift force. The primary advantage of this class of models is that, in addition to predicting the maximum vibration amplitude during lock-in, they are also capable of capturing the distribution profile of vibration amplitudes and response frequencies as a function of wind velocity within the lock-in region.

In the present study, a newly calibrated VIV model based on the Hartlen-Currie lift oscillator equation is proposed, with the aim of serving as a predictive tool for wind turbine tower lock-in events that can be readily integrated into comprehensive, state-of-the-art aeroelastic design frameworks. The constants of the oscillator equation are identified through an optimization procedure designed to accurately reproduce the maximum oscillation amplitude of rigid, elastically supported untapered cylinders at the dimensionless wind velocity where this peak amplitude occurs. Subsequently, model constants variations are introduced across the full range of dimensionless wind velocities to enable the model to reasonably capture the overall amplitude profile within the lock-in region. Target values for the maximum amplitude and corresponding dimensionless wind velocity are derived from two wind tunnel experiments (Belloli et al., 2012; Feng, 1968) conducted on rigid, elastically supported cylinders under different Scruton numbers.

The calibrated oscillator equation is then integrated into NTUA's in-house multibody aeroelastic code, hGAST (Bagherpour et al., 2018; Manolas, 2016; Manolas et al., 2020; Panteli et al., 2022; Riziotis and Voutsinas, 1997), for the prediction of wind turbine tower loads and vibrations in elastic, cantilevered cylinders. The lift equation is used to compute the lift force distribution along the correlation length—defined according to the Eurocode - for a cylindrical, untapered wind turbine tower. Model predictions are validated against wind tunnel measurements (Lupi et al., 2021) of vibration amplitudes for an untapered cylindrical tower with a clamped base and a free top end, undergoing vortex-induced vibrations (VIV) at the natural frequency of its first bending mode. The results show that the model (calibrated based on measurements on

https://doi.org/10.5194/wes-2025-231
Preprint. Discussion started: 8 December 2025

eawe european academy of wind energy
Open Access WIND ENERGY SCIENCE DISCUSSIONS

elastically mounted rigid cylinders) successfully captures the maximum vibration amplitude and the onset wind speed for lock-in. To accurately estimate the range of wind velocities over which lock-in occurs, across a range of Scruton (Sc) numbers, the model needs further calibration based on observations from experimental data of clamped vibrating cylinders in their bending modes. It should be noted that vortex-induced vibrations in higher-order modes (second tower bending mode), as well as the influence of ambient turbulence on the development of the lock-in phenomenon, are not addressed in the present study and are identified as subjects for future research.

The paper is organized as follows. In Section 2, first, the lift-oscillator model and its parameter calibration procedure are introduced (Section 2.1). Next, the calibrated model's performance is assessed against state-of-the-art semi-empirical tools for vortex-induced vibration (VIV) prediction (Section 2.2) followed by the integration of the lift-oscillator model into the existing multi-body solver is then described (Section 2.3). In Section 3 a comparison between the model predictions and experimental measurements on cantilever flexible cylinder are presented whereas Section 4 provides the conclusions of the present work.

2 Methodology

The present work is structured into the following methodological steps:

(a) The two constants of the Hartlen-Currie lift-oscillator model are calibrated using data from two wind tunnel experiments conducted on rigid, untapered, elastically mounted cylinders subjected to crossflow vortex-induced vibrations (VIV). The calibration aims at determining the constant values that yield the target maximum oscillation amplitude at the specific dimensionless velocity where this amplitude occurs within the lock-in region, and across different values of the Sc number. This is achieved through an optimization process using the COBYLA algorithm, as implemented in the "scipy.optimize" module of the SciPy library (SciPy Contributors, 2024). For dimensionless velocities other than the one corresponding to the peak amplitude, a simplified parameter identification approach is employed by assuming a linear decay of the parameters from their values at maximum resonance. This follows the reasoning of Tamura (Tamura, 2020), who argues that parameter selection should not rely solely on curve fitting, but must also respect the physical characteristics of the phenomenon.

(b) The calibrated lift-oscillator model is then integrated within the in-house multibody finite element (FEM) structural solver, hGAST. In this framework, the 3D cantilever cylinder is modeled as a Timoshenko beam, offering a simplified yet robust aeroelastic model for predicting VIV on cantilevered wind turbine tower structures. The Hartlen-Currie lift equation is solved at each timestep for every finite element, in strong coupling with the structural beam equations — an iterative procedure is followed until both the aerodynamic and structural solutions converge. The aerodynamic lift force predicted by the model is distributed along the height of the tower and applied as an external load to the corresponding finite elements. The correlation length, defined as the portion of the tower over which the aerodynamic loads are applied, is incorporated following Eurocode guidelines and depends on the maximum oscillation amplitude. Beyond this correlation length, the external forcing is reduced to zero.

https://doi.org/10.5194/wes-2025-231
Preprint. Discussion started: 8 December 2025

eawe european academy of wind energy
Open Access WIND ENERGY SCIENCE DISCUSSIONS

2.1 The Hartlen-Currie two equation lift-oscillator model

In the following subsections the Hartlen-Currie two equations lift oscillator model is presented along with the calibration procedure for the determination of the constants of the model.

2.1.1 Equations of the model of the elastically mounted rigid cylinder

In the Hartlen–Currie two degrees of freedom (DOF) model, the second-order in time differential equation of motion for an elastically supported rigid cylinder in the direction perpendicular to the inflow velocity (the motion is denoted by the displacement y in Fig. 1) is coupled with a second-order, nonlinear differential equation that governs the dynamic lift coefficient C_L:

$$m\ddot{y} + c\dot{y} + ky = C_L \frac{\rho}{2} U^2 Dl \quad (1)$$

$$\ddot{C}_L - G\left(-\left(\frac{4}{3}\right)\left(\frac{\dot{C}_L}{\omega_s}\right)^2 + C_{L0}\right)\dot{C}_L + \omega_s^2 C_L = -H\,\ddot{y} \quad (2)$$

In (1), m, k and c are the mass of the cylinder and the spring and damping coefficients of its elastic support, D is diameter and l the length of the cylinder, U is the inflow velocity and ρ the density of the fluid. The constants G and H in (2) are free parameters of the model that need to be provided by the user of the model. Furthermore, $\omega_s = 2\pi f_s$ in Eq. (2) is the shedding angular frequency (and f_s the corresponding frequency) of the rigid cylinder (corresponding to the shedding Strouhal number St) and C_{L0} is the lift coefficient variation amplitude (due to vortex shedding) of the rigid cylinder case. Both St and C_{L0} are obtained from experiments on rigid cylinders as functions of the Reynolds number (Re) (Schewe, 1983).

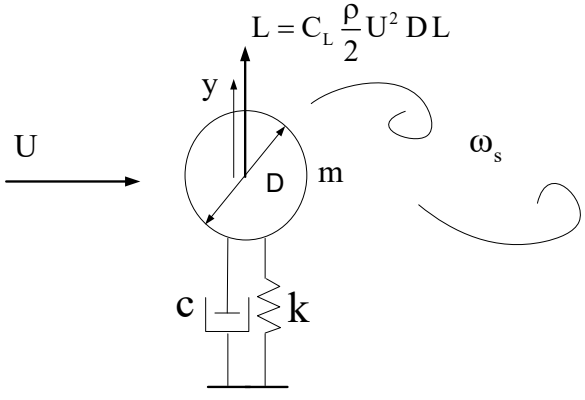

Figure 1: Elastically supported cylinder

Equations (1) and (2) can be expressed in non-dimensional form by introducing the non-dimensional displacement and time parameters η and τ respectively, defined as:

https://doi.org/10.5194/wes-2025-231
Preprint. Discussion started: 8 December 2025

eawe european academy of wind energy
Open Access WIND ENERGY SCIENCE DISCUSSIONS

$$\eta = y/D \quad , \quad \tau = tU/D$$

The non-dimensional equations (1) and (2) are then written:

$$\eta'' + \left(\frac{4}{m^* U^* \pi} Sc\right)\eta' + \left(\frac{4\pi^2}{U^{*2}}\right)\eta = \frac{2C_L}{m^*\pi} \tag{3}$$

$$C_L'' - \left(\frac{GD}{U}\right)\left(-\left(\frac{4}{3}\right)\frac{C_L'^2}{4\pi^2 St^2} + C_{L0}\right)C_L' + 4\pi^2 St^2 C_L = -\left(\frac{HD^2}{U}\right)\eta' \tag{4}$$

Where in (3) and (4), $(\cdot)' = \frac{d}{d\tau}(\cdot)$, $m^* = \frac{4m_{eq}}{\pi\rho D^2}$ is the dimensionless mass ratio of the cylinder, $m_{eq} = m/l$ the linear mass of the cylinder, $U^* = \frac{U}{f_n D}$ is the dimensionless flow velocity, where $f_n = (\omega_n/2\pi) = \sqrt{k/m}/2\pi$ is the natural frequency of the elastic cylinder, $Sc = \frac{4\pi m_{eq}\zeta}{\rho D^2}$ is the dimensionless Sc number, where ζ is the critical damping ratio given by $2\zeta\omega_n = c/m$ and $St = \frac{f_s D}{U}$ is the shedding Strouhal number.

Notably, in (4), the coefficients $\frac{GD}{U}$ and $\left(\frac{HD^2}{U}\right)$ can be replaced by two new constants G' and H', which remain unchanged for a given set of the dimensionless parameters m^*, Sc, U^* and St, independent of the actual values of the dimensional parameters of the problem. The non-dimensional formulation of equations (3) and (4) facilitates the calibration of the model's defining constants, since this process must be carried out only once for a specified set of dimensionless parameters.

It is noted that in the present study we chose to define G' and H' as follows:

$$\mathrm{G}' = \frac{\mathrm{G}}{\omega_s} = \frac{\mathrm{GD}}{\mathrm{U}}\left(\frac{1}{2\pi\ \mathrm{St}}\right) \tag{5}$$

$$H' = \frac{HD}{\omega_s} = \frac{HD^2}{U}\left(\frac{1}{2\pi\ St}\right) \tag{6}$$

It is also worth noting that, for a typical vortex-shedding Strouhal number of 0.2 in the subcritical regime, the dimensionless velocity at which the vortex-shedding frequency of the rigid cylinder matches the natural frequency of the elastically mounted cylinder is $U^* = 5$.

2.1.2 Model constants calibration procedure

The constants G' and H' of the Hartlen-Currie lift-oscillator model are calibrated using data from wind tunnel experiments conducted on rigid, untapered, elastically mounted cylinders subjected to crossflow vortex-induced vibrations (VIV). The calibration procedure is illustrated in Fig 2. Experimental studies provide data on the variation of the maximum vibration amplitude y_{max} with respect to U^*, for different values of the Scruton number. In most cases, experiments are carried out for only one or a limited range of m^* values. As shown in Fig. 2, the ultimate maximum amplitude (onset of VIV) typically

https://doi.org/10.5194/wes-2025-231
Preprint. Discussion started: 8 December 2025

eawe european academy of wind energy
Open Access WIND ENERGY SCIENCE DISCUSSIONS

occurs at U^* values greater than those for which the natural frequency of the elastically mounted cylinder equals the shedding frequency of the rigid cylinder (as noted above, this corresponds to $U^* = 5$ for St=0.2) or at wind velocities exceeding the critical value ($U/U_{crit} > 1$), where U_{crit} is defined by the following expression:

$$St = 0.2 = \frac{f_n D}{U_{crit}}$$

For each available experimental dataset of m^*, Scr and St, an optimization loop is executed using the COBYLA method, as implemented in the Python SciPy package (SciPy Contributors, 2024), to determine the optimal values of the constants G' and H' that yield the target peak amplitude y_{max} at the corresponding U^*_{max}. The differential equations (3) and (4) are numerically integrated in time until resonant oscillations build up. The objective of the optimization procedure is to minimize the difference between the oscillation amplitude obtained for a given pair of constants with the target amplitude. Numerical integration is performed using implicit 2nd order Newmark method as implemented in (Zou et al., 2014). Once the optimal G' and H' are determined for U^*_{max}, a simplified approach is applied to describe their variation for U^* values other than U^*_{max}. The lock-in region is assumed to lie within a specific U^* range $[U^*_{low}, U^*_{high}]$ as indicated by experimental data (that is, the range of U^* over which y_{max} remains significant). It is then assumed that G' and H' (the values determined through the optimization loop) decrease linearly to zero from U^*_{max} towards both U^*_{low} and U^*_{high} as shown in Fig. 2. Through the above procedure, a single set of optimal G' and H' values characterizes each combination of the dimensionless parameters governing the physical problem. This approach eliminates the need for complex optimization simulations across the entire lock-in range, while ensuring that the physical parameters of the problem (extent of lock-in range) are preserved.

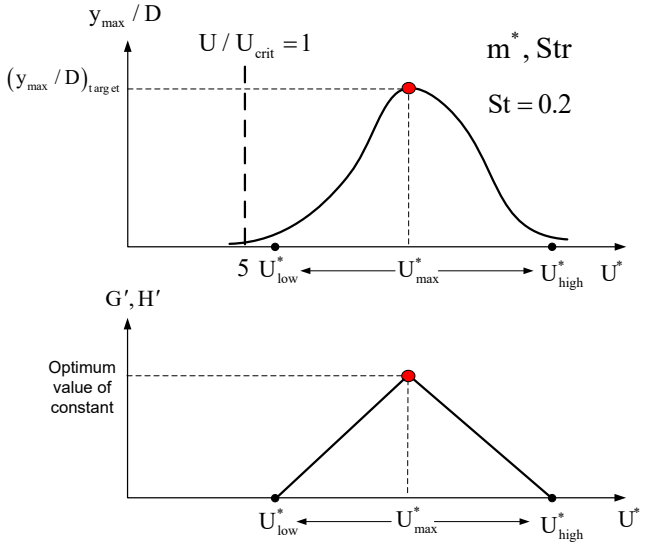

Figure 2: G' and H' calibration process.

https://doi.org/10.5194/wes-2025-231
Preprint. Discussion started: 8 December 2025

In the following sections, the constants of the Hartlen–Currie model are optimized using two distinct experimental datasets for rigid, untapered, elastically supported cylinders. For each experiment, optimization is carried out for a single m^* value, thereby eliminating any potential dependency of the constants on the mass ratio. However, the optimization covers a range of Sc values. It should also be noted that both experiments were conducted within the subcritical Reynolds number regime, where the Strouhal number of vortex shedding is approximately 0.2.

2.2 Model calibration results

Two experimental wind tunnel datasets on VIV of a rigid, untapered, elastically supported cylinder are used to calibrate the parameters of the lift oscillator equation. The first and more recent campaign is by (Belloli et al., 2012) was conducted at POLIMI wind tunnel on a cylinder with diameter $D = 0.2m$, aspect ratio $l/D = 10$, mass ratio $m^* = 170$, at a nominal $Re = 4.6 \times 10^4$ (in the subcritical regime). The vortex shedding Strouhal number of the rigid cylinder at the above conditions was measured $St = 0.18$. Tests are conducted for three values of the Sc number, $Sc = 1.00,\ 4.36,\ 6.67$. The second and older test by (Feng, 1968) was conducted in the wind tunnel at the university of British Columbia on a cylinder with diameter $D = 0.076m$, aspect ratio $l/D = 9$, mass ratio $m^* = 248$ and $Re = 1 \times 10^4 \div 5 \times 10^4$ (again in the subcritical regime). The vortex shedding Strouhal number was measured $St = 0.198$ and the Sc number was varied in the range $Sc = 2.52 \div 7.92$.

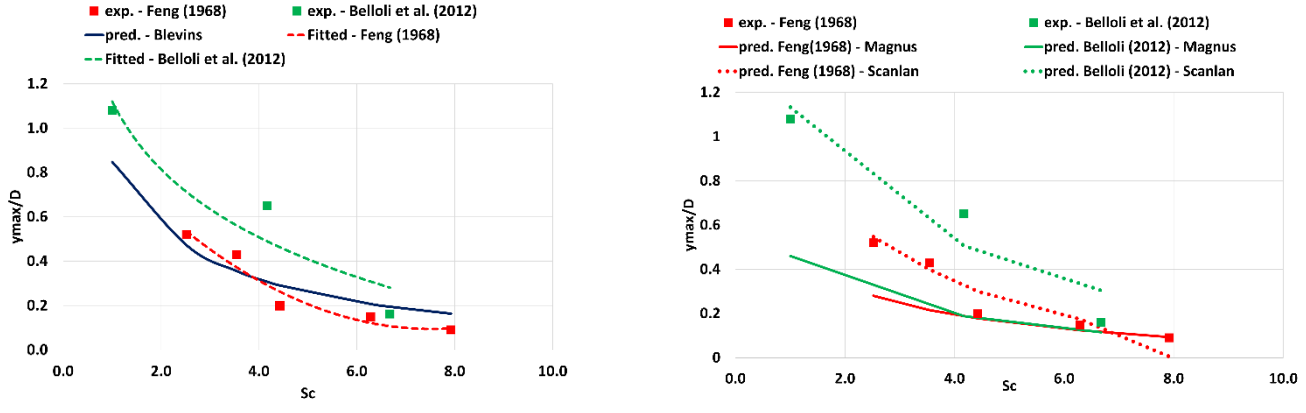

n

(a) (b)

Figure 3: Maximum oscillation amplitude in VIV. Comparison of two wind tunnel tests results with different models from literature.

To demonstrate the predictive capabilities of the analytical model of Blevins (Blevins, 1977) and the one-equation models discussed in the introduction section, the measured data are first compared against the analytical model and the one-equation models proposed by Scanlan (Scanlan, 1981) and Magnus (Magnus et al., 2013). Figure 3 (a) and (b) present the

https://doi.org/10.5194/wes-2025-231
Preprint. Discussion started: 8 December 2025

eawe european academy of wind energy
Open Access WIND ENERGY SCIENCE DISCUSSIONS

measured peak VIV amplitudes from the two experiments as functions of the Scruton number (Sc). In Figure 3 (a), smooth trend lines have been fitted through both experimental datasets, which are then compared with the predictions of the Blevins model. Figure 3 (b) compares the measured data with the predictions of the two one-equation models by Scanlan and Magnus. The governing equations of these models are provided in the Appendix along with a full list of symbols. A comparison of the two experimental datasets shows that the more recent measurements by Belloli et al. (2012) exhibit significantly larger oscillation amplitudes at $Sc = 4.36$, but are in close agreement with Feng's results for higher Sc values ($Sc > 6$). Comparison between model predictions and experimental data reveals that the Blevins model tends to slightly overpredict peak amplitudes at high Sc numbers ($Sc > 6$), while considerably underpredicting them at low Sc values ($Sc \approx 1$). Regarding the one-equation models, the results indicate that Scanlan's model generally provides better agreement with measurements than the Magnus model. The latter offers reasonable peak amplitude predictions at high Sc values but underestimates amplitudes for $Sc < 3$.

In the following, the results of the calibration procedure for the constants of the Hartlen–Currie model are provided. It should be noted that the calibration was carried out using peak amplitudes obtained from the fitted, smooth trendlines, rather than directly from the raw measurement data. This approach minimizes the influence of outliers in the experimental data, such as the anomaly observed in the Belloli test for $Scr = 4.36$.

The range $[U^*_{low}, U^*_{high}]$ within which the parameters G' and H' take non-zero values is defined as [5.5, 9] based on examination of the measured data. In the optimization simulations C_{L0} was taken equal to 0.3, the amplitude value that corresponds to the subcritical regime of the Re number.

In Fig. 4, the predicted by the newly calibrated model peak amplitudes are compared to the measured data. Given that the results of the proposed method rely heavily on the selection of the range $[U^*_{low}, U^*_{high}]$, a simpler alternative of maintaining constant G' and H' values across the entire U* range is also assessed. The constant values used are those obtained from the optimization run at U^*_{max}. For the high Sc number case (Sc = 6.67, representing high damping), both methods accurately capture the dimensionless velocity range of lock-in and the peak oscillation amplitude during VIV. However, maintaining constant G' and H' values leads to a shift of U^*_{max} towards the value that corresponds to $U/U_{crit} = 1$. In contrast, the method with varying G' and H' provides amplitude predictions that align better with the measurements. For the low Sc number case (Sc=1.00, representing low damping), the constant G' and H' method slightly overpredicts the peak amplitude as well as the range of U* for which oscillation amplitudes remain significant. Furthermore, a slight shift of high amplitudes towards lower U* is again observed. On the other hand, the method with varying model constants (denoted as 'Prediction' in the plots) provides a much closer agreement with measurements across the entire U* range.

https://doi.org/10.5194/wes-2025-231
Preprint. Discussion started: 8 December 2025

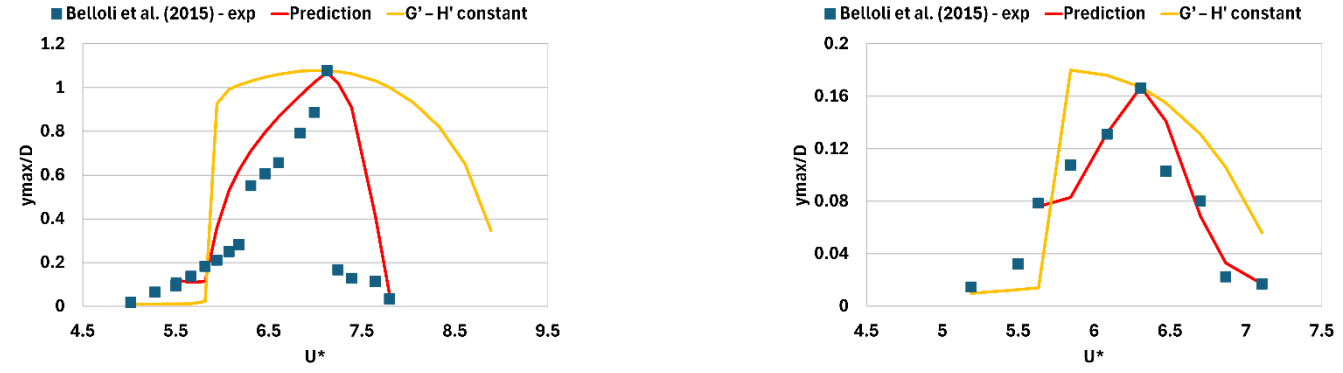

Figure 4: Oscillation amplitudes vs. U*. Calibration of the model constants with measurements from Belloli et al 2012. Predictions correspond to varying and constant G' and F'. Two Sc values addressed (a) Sc=1, (b) Sc=6.67. Mass ratio $\boldsymbol{m^* = 170}$ and $\boldsymbol{Re = 4.6 \times 10^4}$.

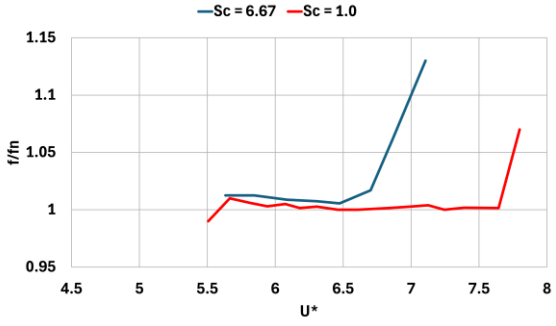

Figure 5: Frequency ratio across VIV zone for two Sc values.

In Fig 5, the dimensionless oscillation frequency for low and high Sc cases is presented. The plateau of the frequency plot at f/fn=1 signifies the occurrence of VIV, where the vortex shedding frequency locks in with the natural frequency, resulting in synchronized vortex shedding and structural vibrations. The extent of this plateau indicates the range of the lock-in, while departure from f/fn=1 indicates the end of lock-in and the subsequent decay of oscillation amplitudes. The lock-in range is noticeably narrower for the higher Scruton number.

For the dataset of (Feng, 1968) the range $[U^*_{low}, U^*_{high}]$ within which the parameters G' and H' take non-zero values is defined as [5, 8] based on examination of the measured data. As in the case of the first test, in the optimization simulations, C_{L0} was taken equal to 0.3.

As shown in Fig. 6, similar to the first test, the varying constants method provides reasonable predictions of the oscillation amplitudes within the lock-in region across all Sc numbers, exhibiting good agreement with the measurements.

https://doi.org/10.5194/wes-2025-231
Preprint. Discussion started: 8 December 2025

eawe european academy of wind energy
Open Access WIND ENERGY SCIENCE DISCUSSIONS

The inability to predict the ultimate maximum amplitude in certain cases (e.g., Sc = 4.43 and 6.29) is attributed to the model constants being optimized based on the peak amplitudes derived from the smooth trend lines in Fig. 3, which sometimes deviate significantly from the measured values. Overall, the varying constants method effectively captures both the amplitude distribution within the lock-in range and the extent of the lock-in region for all Sc values. As in the previous test, maintaining constant G' and H' leads to a shift of U^*_{max} towards lower U* values closer to the U/Ucrit=1 condition.

https://doi.org/10.5194/wes-2025-231
Preprint. Discussion started: 8 December 2025

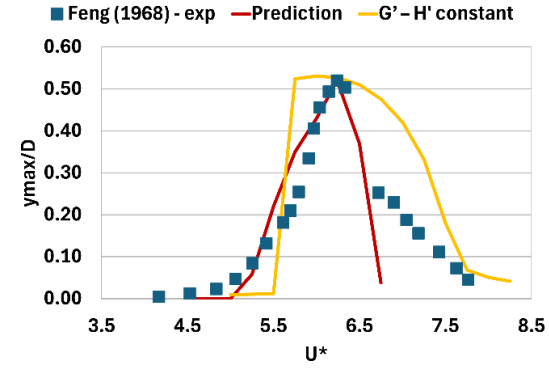

a: Sc = 2.52

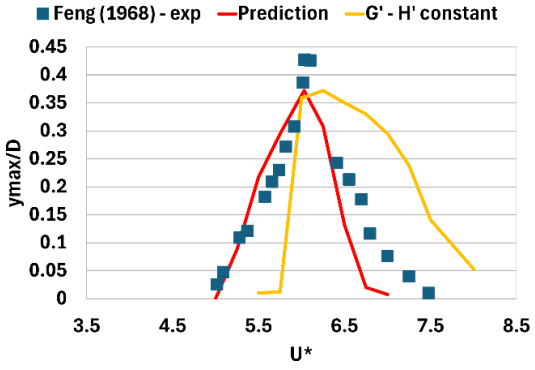

b: Sc=3.55

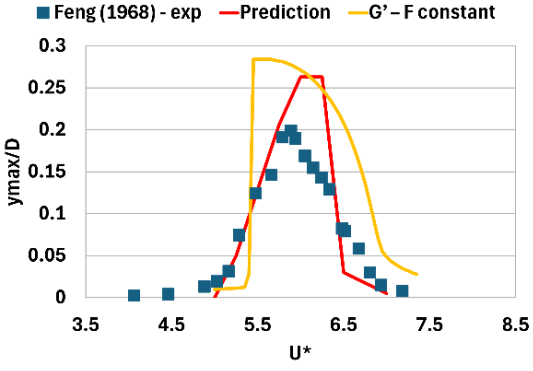

c: Sc=4.43

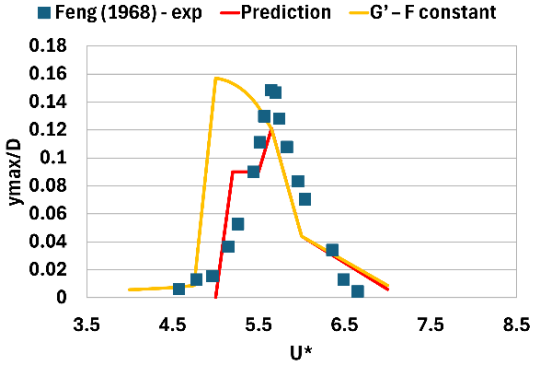

d: Sc=6.28

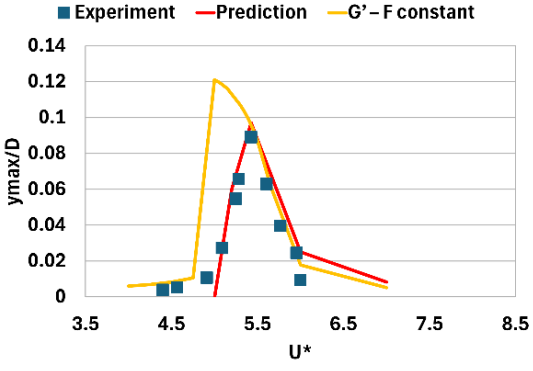

e: Sc=7.92

Figure 6: Oscillation amplitudes vs. U*. Calibration of the model constants with measurements from Feng, 1968. Predictions correspond to varying and constant G' and F'. Scruton numbers range from 2.52 to 7.92. Mass ratio $\boldsymbol{m^* = 248}$ and $\boldsymbol{Re = 1 \times 10^4 \div 5 \times 10^4}$.

https://doi.org/10.5194/wes-2025-231
Preprint. Discussion started: 8 December 2025

eawe european academy of wind energy
Open Access WIND ENERGY SCIENCE DISCUSSIONS

A comparison of the two tests, in terms of the variation of the peak amplitude in VIV as a function of the Sc number (Fig. 3), shows that they yield similar results, apart from the outlier at Sc = 4.43 in the POLIMI test. However, a notable difference between the two experiments lies in the predicted U* value at which the onset of VIV occurs. For all Sc numbers, the POLIMI test consistently provides higher U^*_{max} values, although the two experiments are conducted in the same range of Re (O(10^4)). The main difference between the two experimental campaigns lies in the mass ratio of the cylinders. The POLIMI test was conducted at a lower mass ratio (m*=170) compared to Feng's test (m*=250), which could be partially the explanation of the difference. Despite the aforementioned difference, the constants obtained from the optimization runs for the two datasets exhibit similar trends, as shown in Fig. 7. The value of G'_{max} shows an almost linear decrease with increasing Sc, whereas the opposite behaviour is observed for the H'_{max} constant, which increases linearly with Sc. In Fig. 7, alongside the optimal G'_{max} and H'_{max} values for the two tests, fitted trend lines are also presented. These lines will subsequently serve as envelope curves for determining appropriate constant values to be used in the cantilever tower analysis of section 3.

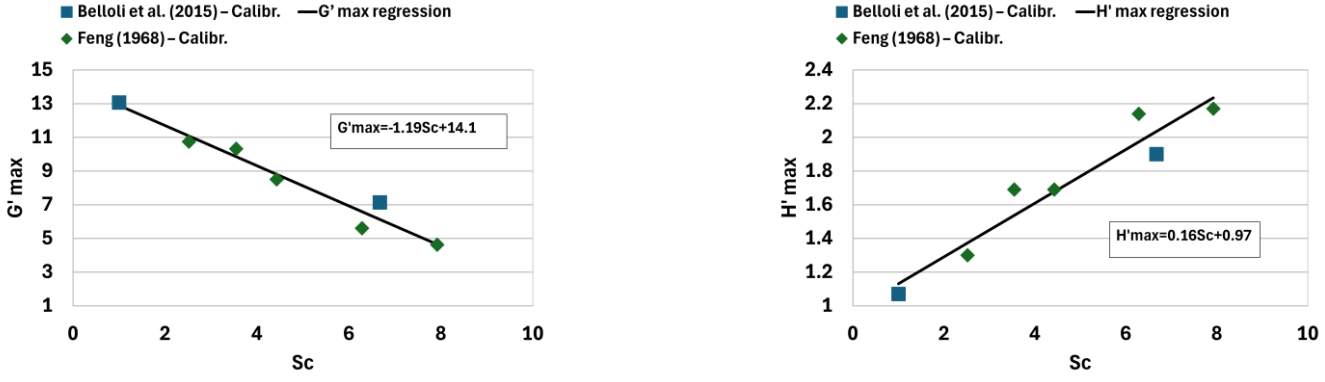

Figure 7: G'_{max} and H'_{max} across the range of Scruton numbers tested.

2.3 Implementation of the Hartlen-Currie lift equation in hGAST

The lift-oscillator model presented and calibrated in sections 2.1-2.2 is integrated within the in-house multibody finite element (FEM) hydro-servo-aero-elastic solver and stability analysis tool, hGAST (Manolas et al., 2020; Riziotis et al., 2008). hGAST, models the full wind turbine as a multi-component dynamic system, having as components the blades, the drive train and the tower. The components are assembled into the full configuration on the basis of the multibody formulation. It consists of considering each component separately from the others but subjected to specific free-body kinematic and loading conditions, that are imposed at the connection points of the components. The multibody formulation is also extended to the level of the components (e,g. blades and tower), which can be divided into a number of sub-bodies connected to each other through similar kinematic and dynamic constraint conditions. In this way geometric non-linearities related to large deflections are taken into account. All flexible components (blades, drive train and tower) are modelled as Timoshenko beam structures subjected to bending, torsion and tension and approximated with the Finite Element Method

https://doi.org/10.5194/wes-2025-231
Preprint. Discussion started: 8 December 2025

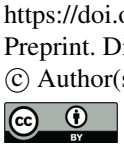

eawe european academy of wind energy
Open Access WIND ENERGY SCIENCE DISCUSSIONS

(FEM). An enhanced Blade Element Momentum Theory (BEMT) model approximates the aerodynamics of the rotor taking into account mean inflow characteristics such as yaw, shear, veer and inclination as well as turbulent fluctuations. Viscous effects, unsteady airfoil aerodynamics and dynamic stall are taken into account using the ONERA model. In the standard version of hGAST, the aerodynamic loading of the tower consists only of a steady drag force acting on every element of the tower in the direction of the incoming local flow (drag coefficient is defined as function of the local Re number). The aerodynamic and structural dynamic problems are implicitly coupled (iteration are performed between the two problems until convergence of both is achieved). The integration of the system dynamic equations in time is performed using the Newmark 2nd order scheme.

In the framework developed in the present work, the 3D cantilever cylinder is modeled as a collection of interconnected linear Timoshenko sub-bodies, offering a simplified yet robust aeroelastic model for predicting VIV on cantilevered wind turbine tower structures. Alongside the steady drag force acting in the direction of the relative wind, a lift force perpendicular to its direction is added, calculated through the solution of the Hartlen-Currie lift equation (see Figure 8). The lift oscillator equation is solved at each timestep of the simulation for every sub-body of the tower, in successive iterations until both the aerodynamic and structural dynamic solutions converge. The aerodynamic lift force predicted by the model is distributed along the height of the tower and applied as an external load to the corresponding finite elements. The correlation length, defined as the portion of the tower over which the aerodynamic loads are applied, is incorporated following Eurocode guidelines (see the Appendix) and depends on the maximum oscillation amplitude. Beyond this correlation length, the external forcing is reduced to zero.

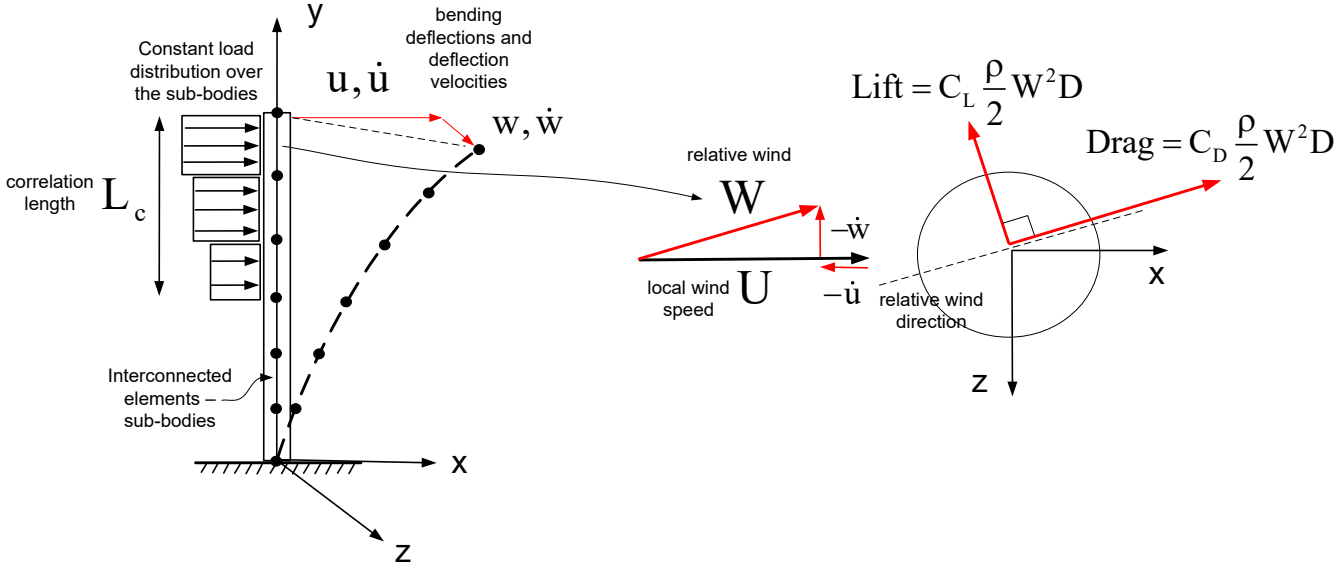

Figure 8: Tower aerodynamic loads calculation in hGAST.

https://doi.org/10.5194/wes-2025-231
Preprint. Discussion started: 8 December 2025

eawe european academy of wind energy
Open Access WIND ENERGY SCIENCE DISCUSSIONS

3 VIV predictions on a cantilever cylinder

The calibrated Hartlen–Currie model (calibration based on elastically supported rigid cylinder) is validated against an experimental setup consisting of a cantilevered cylinder exposed to low Reynolds number flow ($Re \approx 20000$), replicating the configuration of Lupi et al. (Lupi et al., 2021). In the experiments, different cylinder models are used for testing different Sc conditions, which are also replicated in the simulations presented herein. The main geometric and structural parameters of the cylinder models tested in the wind tunnel are summarized in Table 1. The simulations are conducted employing calibration parameters obtained from Belloli et al. 2012, corresponding to the experimental dataset that exhibited the closest agreement with Lupi's cantilever tower experiment regarding the values U^*_{max} and its variation with Sc. Nevertheless, differences are expected to be marginal in case the calibration parameters obtained from Feng et al. 1968 were considered.

As shown in Fig. 9b,c, and Fig. 10 the model accurately reproduces the maximum tip displacement for the two higher Sc values ($Sc = 5.18$ and $Sc = 7.02$). However, for $Sc = 2.94$, it overpredicts the displacement by approximately 55%. The wind tunnel experimental results presented in Fig. 3 indicate that, for $Sc \approx 3$, the maximum vibration amplitude in the VIV response of an elastically supported rigid cylinder lies in the range of 0.4–0.5, which is significantly higher than the corresponding values reported in Lupi's experiment for the same Sc. This clearly demonstrates that the present results are governed by the experimental dataset used for model calibration. Furthermore, as indicated by the γ coefficient in Blevins' model (see Appendix), which exceeds unity in the case of a cantilever beam, the maximum VIV tip amplitudes of a cantilever beam are expected to be higher than those of an elastically supported rigid cylinder. In addition, the predicted lock-in region is well captured for $Sc = 2.94$, whereas it is considerably underpredicted for higher Sc values. This outcome also reflects the influence of the rigid-cylinder measurements used for calibration, which show a narrower lock-in region that decreases with increasing Sc. In contrast, for the cantilever case, increasing Sc primarily reduces the maximum displacement amplitude, while the lock-in range appears to remain essentially unchanged.

The underprediction of the lock-in region highlights a limitation: calibrations based solely on rigid-cylinder data are sufficient for estimating maximum amplitudes but inadequate for realistic cantilever elastic structures, such as wind turbine towers. The lock-in zone width depends on the rate at which the defining parameters vary towards zero from their calibrated value at U^*_{max}. To explore this sensitivity, two additional parameter ranges were tested. The baseline calculation used $U^* \in [5.5,9]$ (in accordance with Belloli's wind tunnel tests), while two alternative ranges of $U^* \in [4.5,10]$ and $U^* \in [5,10]$ are also considered. Fig. 9b compares the model response across the lock-in range for these different parameter zones. The model consistently links the predicted lock-in width to the span of the chosen parameter range. Specifically, a faster increase or decrease in the calibration constants shifts the predicted onset of VIV to higher reduced velocities and produces a much steeper slope, failing to capture the gradual buildup of oscillations. In contrast, the decaying part of the oscillations (at higher U* values) appears largely unaffected by the choice of parameter range.

https://doi.org/10.5194/wes-2025-231
Preprint. Discussion started: 8 December 2025

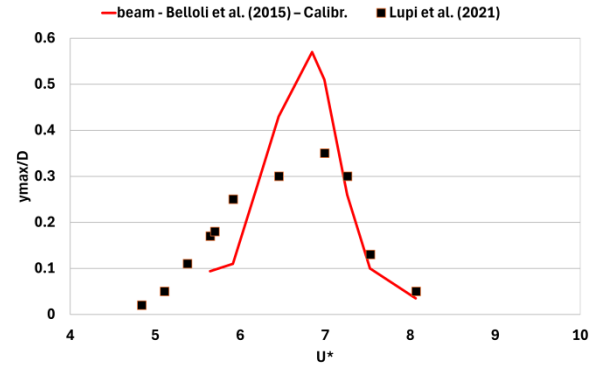

a. Sc=2.94

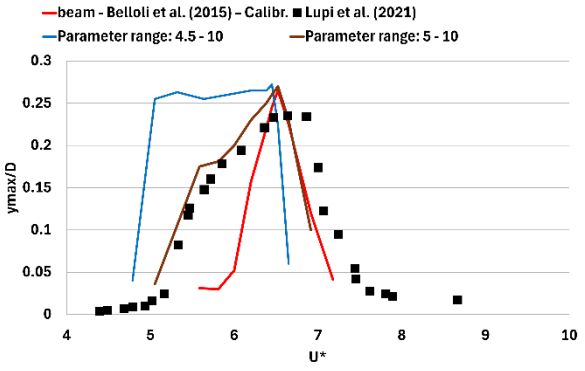

b. Sc=5.18

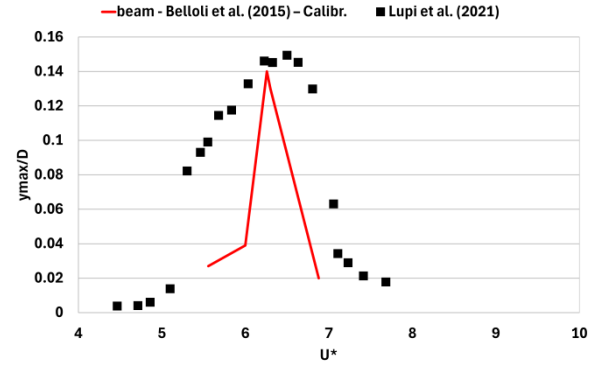

c. Sc=7.02

Figure 9: Oscillation amplitudes vs. U* for the cantilever tower.

355

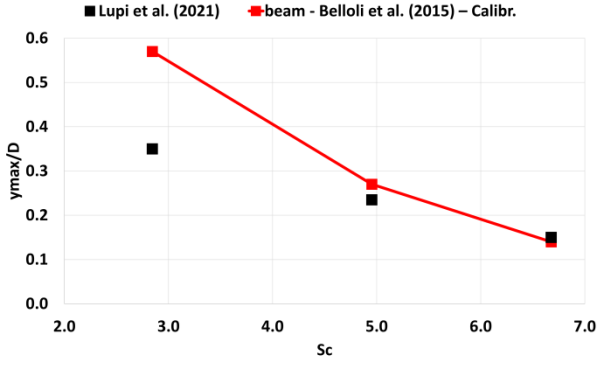

Figure 10: Oscillation amplitudes vs. Sc for the cantilever tower.

https://doi.org/10.5194/wes-2025-231
Preprint. Discussion started: 8 December 2025

eawe european academy of wind energy
Open Access WIND ENERGY SCIENCE DISCUSSIONS

Table 1: Geometric and structural parameters of the cylinder models tested in the wind tunnel

Configuration	**1**	**2**	**3**
Height (mm)	775	775	775
Diameter (mm)	50	50	50
Natural Frequency (Hz)	20.02	15.38	13.18
Equivalent mass (kg/m)	0.2311	0.4311	0.6027
Structural damping ratio	0.0030	0.0028	0.0027
Scruton number	2.94	5.18	7.02

4 Conclusions

The study presents the calibration and validation of a predictive engineering model for vortex-induced vibrations (VIV) in wind turbine towers, based on the Hartlen–Currie lift oscillator formulation. The governing equations of the lift oscillator model are expressed in a non-dimensional form to facilitate the calibration of the model's defining parameters. In this formulation, calibration is required only for specific sets of the problem's characteristic dimensionless parameters.

Model parameters are calibrated using experimental data obtained from elastically mounted, rigid, untapered cylinders, enabling accurate prediction of vibration amplitudes and onset wind speeds U^*_{max} associated with lock-in phenomena. Integration of the calibrated model into a multibody aeroelastic solver demonstrates its capability to simulate VIV responses in elastic cantilevered cylinders, representing configurations relevant to real wind turbine towers. Comparisons with wind tunnel measurements show that the proposed model successfully predicts the maximum vibration amplitudes and the onset velocity of VIV. However, it tends to underestimate the width of the lock-in velocity range, particularly at higher Scruton numbers. This discrepancy does not indicate a shortcoming of the model itself, as it can be mitigated by refining parameter calibration using direct VIV wind tunnel measurements of the cantilever tower.

Furthermore, both the calibration and validation of the model rely on low-Reynolds-number wind tunnel data, significantly lower than those expected under full-scale wind turbine operating conditions, due to the lack of high-Reynolds-number experimental data. This does not constitute a limitation of the current work, as the model can be readily updated when such high-Reynolds-number data become available.

The present approach focuses on the first bending mode, while neglecting higher-order modes and the influence of ambient turbulence—factors identified as directions for future research. Overall, the calibrated Hartlen–Currie model provides a robust predictive tool that can be integrated into comprehensive aeroelastic design frameworks, enhancing the reliability and fatigue assessment of wind turbine towers subjected to vortex shedding excitation.

https://doi.org/10.5194/wes-2025-231
Preprint. Discussion started: 8 December 2025

eawe european academy of wind energy
Open Access WIND ENERGY SCIENCE DISCUSSIONS

Data availability

Data used to calibrate the model has been obtained from literature. More details concerning the codes used and the experimental data can be found in the corresponding cited publications.

Author contribution

D Vlastos and V Riziotis planned the research; the code was developed by D Vlastos, V Riziotis and N Spyropoulos; D Vlastos, N Tzimi, G.A. Trampa performed the calculations; D Vlastos and V Riziotis wrote the manuscript; D Manolas and N Spyropoulos reviewed the manuscript.

Competing interests

The authors declare that they have no conflict of interest.

Appendix A: List of symbols

y	Crosswind tower elastic displacement
D	Tower diameter
l	Length of the cylinder
U	Inflow velocity
ρ	Air density
$\eta = y/D$	Nondimensional crosswind tower elastic displacement
$\tau = tU/D$	Nondimensional time parameter
m, c, k	Mass, damping and stiffness of elastically supported rigid cylinder
$m_{eq} = m/l$	Equivalent cylinder mass
ζ	Damping ratio
$\omega_s = 2\pi f_s$	Vortex shedding frequency and angular frequency of the rigid cylinder
$\omega_n = 2\pi f_n$	Natural frequency and angular frequency of the elastic cylinder
G, H	Constants of the Hartlen–Currie model
$\mathrm{G}' = \frac{\mathrm{G}}{\omega_s}, \mathrm{H}' = \frac{\mathrm{HD}}{\omega_s}$	Dimensionless constants of the Hartlen–Currie model
C_L	Lift coefficient of the cylinder
C_{L0}	Lift coefficient variation amplitude due to vortex shedding of the rigid cylinder case
$m^* = \frac{4m_{eq}}{\pi\rho D^2}$	Dimensionless mass ratio

https://doi.org/10.5194/wes-2025-231
Preprint. Discussion started: 8 December 2025

eawe european academy of wind energy
Open Access WIND ENERGY SCIENCE DISCUSSIONS

$U^* = \frac{U}{f_n D}$	Dimensionless flow velocity
U^*_{max}	Nondimensional VIV onset flow velocity
$[U^*_{low}, U^*_{high}]$	Nondimensional velocities lock-in range
$Re = \mathrm{UD}/\nu$	Reynolds number
$St = \frac{f_s D}{U}$	Strouhal number
$Sc = \frac{4\pi m_{eq}\zeta}{\rho D^2}$	Scruton number
U_{crit}	Critical inflow velocity - corresponding to the shedding St number of the rigid cylinder

Appendix B: Blevins model

In (Blevins, 1977) model, the peak amplitude during VIV is approximated by the following analytical expression, given as a function of the Sc and St numbers:

$$Ay = 0.07 D\gamma \frac{\sqrt{0.3 + \frac{0.72}{(1.9 + Sc)St}}}{(1.9 + Sc)St^2}$$

In the equation above, γ is a constant used to distinguish between different types of structures and supports. For a rigid cylinder, γ = 1, whereas, for example, for the first mode of a cantilever beam, γ = 1.305.

Appendix C: Eurocode model

The Eurocode (European Committee for Standardization (CEN), 2005), approximates the maximum oscillation amplitude during VIV through the following analytical expression as function of the Sc and St numbers:

$$\frac{y_{max}}{D} = \frac{1}{St^2}\frac{1}{Sc} K K_w c_{lat}$$

where c_{lat} is the lateral force coefficient defined in standard as function of the Re, while K_w (the effective correlation length factor) and K (the effective mode shape factor) are given by:

$$K_w = \frac{\Sigma_{j=1}^{n} \int_{L_{cj}} |\varphi_{yi}(s)| ds}{\Sigma_{j=1}^{m} \int_{L_j} |\varphi_{yi}(s)| ds} \quad , \quad K = \frac{\Sigma_{j=1}^{m} \int_{L_j} |\varphi_{yi}(s)| ds}{4\pi \Sigma_{j=1}^{m} \int_{L_j} \varphi_{yi}^2(s)\, ds}$$

and φ_{yi} the i-th bending mode shape in the cross flow direction that is excited by the vortex shedding, L_j is the length of the structure between two nodes (see Fig. C1); for cantilevered structures it is equal to the height of the structure, L_{cj} is the

https://doi.org/10.5194/wes-2025-231
Preprint. Discussion started: 8 December 2025

eawe european academy of wind energy
Open Access WIND ENERGY SCIENCE DISCUSSIONS

correlation length as defined in Fig. C1, n is the number of regions where vortex excitation occurs at the same time and m is the number of antinodes of the vibrating structure in the considered i-th mode shape φ_{yi}.

The effective correlation lengths L_{cj} are defined in Table C1.

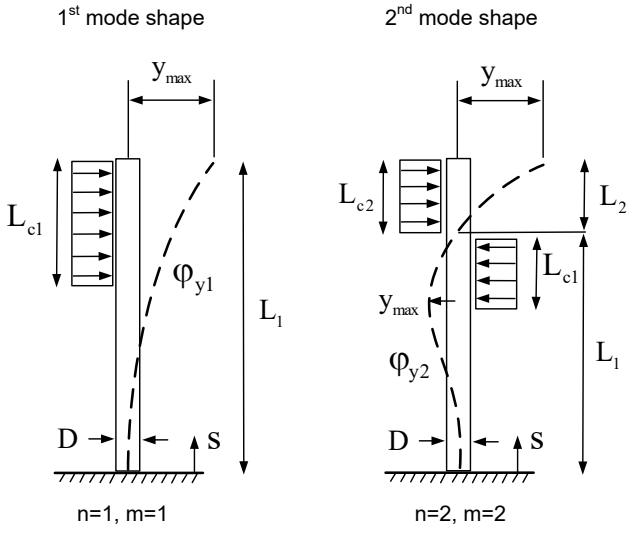

Figure C1: Definition of the correlation lengths in the case of the 1st and 2nd modes of a cantilever beam.

Table C1: Definition of correlation length as function of the maximum oscillation amplitude on either side of the antinode of the mode shape.

yj_{max}	L_{cj}/D
< 0.1	6
0.1 to 0.6	$4.8+12yj_{max}$
> 0.6	12

Appendix D: Scanlan model

The (Scanlan, 1981) one equation model provides the maximum oscillation amplitude of a rigid, elastically supported cylinder of Fig. 1 in the cross flow direction (single DOF of motion y) through the solution of the second order dynamic equation:

$$m\ddot{y} + c\dot{y} + ky = \frac{\rho}{2}U^2 Dl\left(H_1\left(1-\varepsilon\left(\frac{y}{D}\right)^2\right)\frac{\dot{y}}{U} + H_2\frac{y}{D} + C_{L0}\,sin(\omega_s t)\right)$$

The constants H_1, H_2 and ε in the right hand side of the equations are free parameters of the model that need to be specified by the user of the model. The additional stiffness term related to the constant H_2 can be neglected as it is small compared

https://doi.org/10.5194/wes-2025-231
Preprint. Discussion started: 8 December 2025

eawe european academy of wind energy
Open Access WIND ENERGY SCIENCE DISCUSSIONS

with the aerodynamic damping terms related to H_1. H_1 and ε, in turn, are determined from the experimental observation of two resonant response amplitudes $y_{max\,1}$ and $y_{max\,2}$ (or predictions of any analytical model), for two damping ratio values ζ_1 and ζ_2 and the corresponding Scruton numbers, Sc_1 and Sc_2. It can be readily shown (see (Scanlan, 1981)for derivation details) that:

$$H_1 = \frac{8\pi mSt(\zeta_2 y_{max\,1}^2 - \zeta_1 y_{max\,2}^2)}{\rho D^2 (y_{max\,1} - y_{max\,2})} \quad , \quad \varepsilon = \frac{4(\zeta_2 - \zeta_1)D^2}{\zeta_2 y_{max\,1}^2 - \zeta_1 y_{max\,2}^2}$$

Appendix E: Magnus model

The Magnus one equation model (Magnus et al., 2013) provides the maximum oscillation amplitude of a rigid, elastically supported cylinder of Fig. 1 in the cross flow direction (single DOF of motion y) through the solution of the second order dynamic equation:

$$m\ddot{y} + 2m\omega_n \rho D^2 \left(\frac{Scr}{4\pi} - K_a\right)\dot{y} + ky = \frac{\rho}{2} U^2 Dl\ C_{L0}\ sin(\omega_s t)$$

The aerodynamic damping parameter K_a after (Lupi et al., 2018) is expressed as an exponential function of the standard deviation of the oscillations σ_y in VIV:

$$K_a = a \frac{exp\left(-b\frac{\sigma_y}{D}\right)}{\left(\frac{\sigma_y}{D}\right)^c}$$

where, the constants a, b, c are calibrated using experimental data and they are taken equal to:

$$a = 0.3475, \quad b = 5.808, \quad c = 0.3582$$

References

Bagherpour, Tohid., Li, X. M., Manolas, D. I., and Riziotis, V. A.: Modeling of material bend-twist coupling on wind turbine blades, Compos. Struct., 193, 237–246, https://doi.org/10.1016/j.compstruct.2018.03.071, 2018.

Basu, R. I. and Vickery, B. J.: Across-wind vibrations of structure of circular cross-section. Part II. Development of a mathematical model for full-scale application, J. Wind Eng. Ind. Aerodyn., 12, 75–97, https://doi.org/10.1016/0167-6105(83)90081-8, 1983.

Belloli, M., Giappino, S., Muggiasca, S., and Zasso, A.: Force and wake analysis on a single circular cylinder subjected to vortex induced vibrations at high mass ratio and high Reynolds number, J. Wind Eng. Ind. Aerodyn., 103, 96–106, https://doi.org/10.1016/j.jweia.2012.03.005, 2012.

https://doi.org/10.5194/wes-2025-231
Preprint. Discussion started: 8 December 2025

Blevins, R. D.: Flow Induced Vibration, Van Nostrand Reinhold Company, New York, 1977.

European Committee for Standardization (CEN): Eurocode 1: Actions on structures — Part 1-4: General actions — Wind actions, European Committee for Standardization (CEN), 2005.

Feng, C. C.: The measurement of vortex induced effects in flow past stationary and oscillating circular and D-section cylinders, https://doi.org/10.14288/1.0104049, 1968.

Fernandez-Aldama, R., Lopez-Garcia, O., Cuerva-Tejero, A., Gallego-Castillo, C., and Avila-Sanchez, S.: A comparison of vortex shedding models applied to wind turbine tower dynamics, INTERNATIONAL CONFERENCE OF COMPUTATIONAL METHODS IN SCIENCES AND ENGINEERING ICCMSE 2022, Virtual Conference, 110007, https://doi.org/10.1063/5.0193302, 2024.

Hartlen, R. T. and Currie, I. G.: Lift-oscillator model of vortex-induced vibration, J. Eng. Mech. Div. ASCE, 96, 577–591, 1970.

Horcas, S. G., Sørensen, N. N., Zahle, F., Pirrung, G. R., and Barlas, T.: Vibrations of wind turbine blades in standstill: Mapping the influence of the inflow angles, Phys. Fluids, 34, https://doi.org/10.1063/5.0088036, 2022.

Lupi, F., Niemann, H.-J., and Höffer, R.: Aerodynamic damping model in vortex-induced vibrations for wind engineering applications, J. Wind Eng. Ind. Aerodyn., 174, 281–295, https://doi.org/10.1016/j.jweia.2018.01.006, 2018.

Lupi, F., Höffer, R., and Niemann, H.-J.: Aerodynamic damping in vortex resonance from aeroelastic wind tunnel tests on a stack, J Wind Eng Ind Aerodyn, 208, 104438, 2021.

Magnus, K., Popp, K., and Sextro, W.: Schwingungen: Physikalische Grundlagen und mathematische Behandlung von Schwingungen, Springer Fachmedien Wiesbaden, https://doi.org/10.1007/978-3-8348-2575-9, 2013.

Manolas, D. I.: Hydro-Aero-Elastic Analysis of Offshore Wind Turbines, https://doi.org/10.26240/HEAL.NTUA.2154, 22 February 2016.

Manolas, D. I., Riziotis, V. A., Papadakis, G. P., and Voutsinas, S. G.: Hydro-Servo-Aero-Elastic Analysis of Floating Offshore Wind Turbines, Fluids, 5, 200, https://doi.org/10.3390/fluids5040200, 2020.

Manolas, D. I., Chaviaropoulos, P. K., and Riziotis, V. A.: Assessment of Vortex Induced Vibrations on wind turbines, J. Phys. Conf. Ser., 2257, 012011, https://doi.org/10.1088/1742-6596/2257/1/012011, 2022.

Panteli, A. N., Manolas, D. I., Riziotis, V. A., and Spiliopoulos, K. V.: Comparative study of two geometrically non-linear beam approaches for the coupled wind turbine system, J. Wind Eng. Ind. Aerodyn., 231, 105231, https://doi.org/10.1016/j.jweia.2022.105231, 2022.

Riziotis, V. A. and Voutsinas, S. G.: GAST: A general aerodynamic and structural prediction tool for wind turbines, in: Proceedings of the EWEC Conference, Dublin Castle, Ireland, 448–452, 1997.

Riziotis, V. A., Politis, E. S., Voutsinas, S. G., and Chaviaropoulos, P. K.: Stability analysis of pitch-regulated, variable-speed wind turbines in closed loop operation using a linear eigenvalue approach, Wind Energy, 11, 517–535, https://doi.org/10.1002/we.276, 2008.

Scanlan, R. H.: State-of-the-art methods for calculating flutter, vortex-induced, and buffeting response of bridge structures, United States. Department of Transportation. Federal Highway Administration …, 1981.

https://doi.org/10.5194/wes-2025-231
Preprint. Discussion started: 8 December 2025

Schewe, G.: On the force fluctuations acting on a circular cylinder in crossflow from subcritical up to transcritical Reynolds numbers, J Fluid Mech, 133, 265–285, 1983.

SciPy Contributors: COBYLA — Constrained Optimization BY Linear Approximations, SciPy, 2024.

Tamura, Y.: Mathematical models for understanding phenomena: Vortex-induced vibrations, Jpn. Archit. Rev., 3, 398–422, https://doi.org/10.1002/2475-8876.12180, 2020.

Veers, P., Bottasso, C. L., Manuel, L., Naughton, J., Pao, L., Paquette, J., Robertson, A., Robinson, M., Ananthan, S., Barlas, T., Bianchini, A., Bredmose, H., Horcas, S. G., Keller, J., Madsen, H. A., Manwell, J., Moriarty, P., Nolet, S., and Rinker, J.: Grand challenges in the design, manufacture, and operation of future wind turbine systems, Wind Energy Sci., 8, 1071–1131, https://doi.org/10.5194/wes-8-1071-2023, 2023.

Zou, F., Riziotis, V. A., Voutsinas, S. G., and Wang, J.: Analysis of vortex-induced and stall-induced vibrations at standstill conditions using a free wake aerodynamic code: Analysis of vortex-induced and stall-induced vibrations at standstill, Wind Energy, 18, 2145–2169, https://doi.org/10.1002/we.1811, 2014.